Shear Yielding and Shear Jamming of Dense Hard Sphere Glasses

Pierfrancesco Urbani[1] and Francesco Zamponi[2]

[1]*Institut de physique théorique, Université Paris Saclay, CNRS, CEA, F-91191 Gif-sur-Yvette, France*
[2]*Laboratoire de Physique Théorique, ENS & PSL University, UPMC & Sorbonne Universités, UMR 8549 CNRS, 75005 Paris, France*

We investigate the response of dense hard sphere glasses to a shear strain in a wide range of pressures ranging from the glass transition to the infinite-pressure jamming point. The phase diagram in the density-shear strain plane is calculated analytically using the mean-field infinite-dimensional solution. We find that just above the glass transition, the glass generically yields at a finite shear strain. The yielding transition in the mean-field picture is a spinodal point in presence of disorder. At higher densities, instead, we find that the glass generically jams at a finite shear strain: the jamming transition prevents yielding. The shear yielding and shear jamming lines merge in a critical point, close to which the system yields at extremely large shear stress. Around this point, highly nontrivial yielding dynamics, characterized by system-spanning disordered fractures, is expected.

Introduction.—The response of glasses to a shear strain is extremely complex and has always been the subject of much interest for fundamental and technological reasons [1–5]. While at small enough strains, the solid responds elastically, at moderate strains, the response is characterized by small intermittent drops of the shear stress. At larger strains, the stress drops abruptly when the glass yields. Above yielding, the stress remains approximately constant upon increasing strain, and the system flows [4,5]. For soft interaction potentials, it has been established that both low-stress intermittency and large-stress flow are due to "plastic" events at which small regions of the material—called "shear transformations"—fail under stress [2,4,6,7]. The energy relaxed by the failure is propagated elastically through the system, leading to failure in other regions. The stress-strain curves can be well described in the flow regime by elasto-plastic models, which describe mesoscopically the coupling between failing plastic regions [8–11], and the plastic regions themselves have been identified quite precisely in numerical simulations [6,7].

The situation is quite different for dense hard sphere glasses, which are good models of colloidal and granular glasses. These solids, due to the hard sphere constraints, are characterized by a critical "random close packing" or "jamming" density at which a rigid isostatic network of particle contacts emerges, inducing a divergence of the pressure [12–14]. Around the jamming point, due to the emergent contact network, perturbing a particle leads to a macroscopic rearrangement of the whole solid [15–17]: continuum elasticity breaks down [18–21], and solid dynamics are characterized by system-spanning avalanches during which the system relaxes along strongly delocalized soft modes [21–23]. Clearly, in this regime the "shear transformations" picture becomes inappropriate.

The aim of this Letter is to characterize the response of a dense hard sphere glass to a static shear strain (i.e., in the regime where the solid responds by a static stress, without flowing) all the way from the glass transition to the jamming regime, within a mean-field approach. We find that at lower densities, slightly above the glass transition, the hard sphere glass responds in a way similar to soft particle glasses: an elastic regime is followed by an intermittent regime before the system yields ("shear yielding"). At larger densities, close to jamming, the situation is radically different. Before yielding, a jamming transition happens due to shear: at the transition, a rigid network of contacts is formed and the pressure diverges ("shear jamming"). The shear jamming transition is in the same universality class of the jamming transition at zero shear [24,25], and it is characterized by nontrivial critical exponents that appear in the interparticle force and gap distributions [15,26,27]. Most importantly, the shear yielding and shear jamming lines merge in a critical point. Around this point, because the system yields at extremely large (diverging) pressure and shear stress in a regime of incipient jamming, we expect highly nontrivial yielding dynamics, characterized by system-spanning disordered fractures.

Glass preparation protocol.—We consider a system of N identical d-dimensional hard spheres in the thermodynamic limit at constant number density ρ and volume fraction φ. We consider the limit $d \to \infty$, with constant $\hat{\varphi} = 2^d \varphi/d$, in which the liquid and glass properties can be computed exactly within the mean-field random first order transition scenario [28,29]. For hard spheres, the infinite dimensional limit usually provides qualitatively good predictions for the phase diagram of low-dimensional systems [29], especially around jamming [26], and finite-dimensional effects can be studied through numerical simulations [27,30]. Also, for $d > 3$, polydispersity is not needed, as monodisperse hard spheres are a very good glass-forming system [31,32].

During a slow cooling of a liquid, the relaxation time scale $\tau_\alpha(\hat{\varphi})$ becomes extremely large around the mode-coupling density $\hat{\varphi}_d$, but one can still equilibrate up to quite larger values of $\hat{\varphi}$, either by brute force [33] or by means of smart numerical algorithms [34–37] and smart experimental protocols [38]. Once equilibration at some $\hat{\varphi}_g > \hat{\varphi}_d$ has been achieved, one can focus on time scales $\tau_{\exp} \ll \tau_\alpha(\hat{\varphi}_g)$ in such a way that the system remains confined in the glass state selected in equilibrium at $\hat{\varphi}_g$.

In the mean-field limit $d \to \infty$, the liquid relaxation time diverges above $\hat{\varphi}_d$, and the dynamics is completely arrested [28,39,40]. The separation of time scales thus becomes very sharp as $\tau_{\exp} \ll \tau_\alpha(\hat{\varphi}_g) \to \infty$. The "state following" formalism is designed to describe this regime [41–43] in which a typical equilibrium configuration selects a long-lived glass basin, which is then adiabatically followed upon increasing the density $\hat{\varphi} \geq \hat{\varphi}_g$ and applying a shear strain γ [29,44,45]. In particular, the method gives the reduced pressure $p = \beta P / \rho$ and shear stress $\sigma = \beta \Sigma$ of the glass.

The pressure-density equation of state in absence of shear has been studied in [44,45] (Fig. 1). We focus on a liquid compression that remains in equilibrium until $\hat{\varphi}_g = 8 > \hat{\varphi}_d \approx 4.8$ (this is representative of a typical situation), and we follow the corresponding glass in a restricted equilibrium. This glass undergoes a Gardner phase transition to a marginally stable state [26,29,44,45], and then
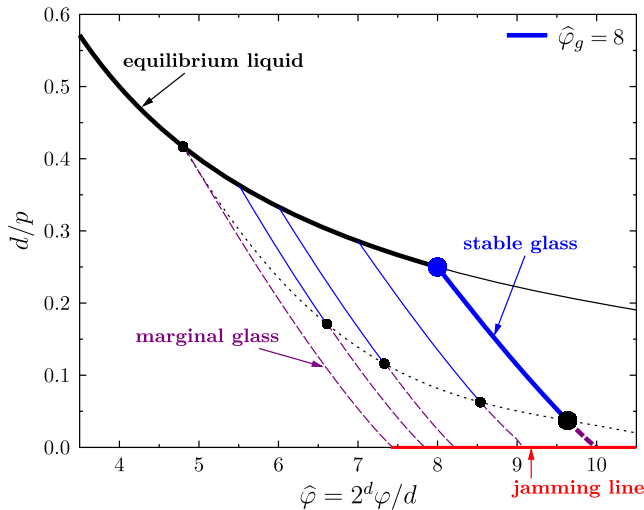

FIG. 1. Inverse reduced pressure d/p versus packing fraction $\hat{\varphi} = 2^d \varphi / d$ (both scaled to remain finite for $d \to \infty$) during a slow compression [44,45]. The liquid EOS is $d/p = 2/\hat{\varphi}$. The dynamical transition $\hat{\varphi}_d$ is marked by a black dot. We focus on a liquid slowly compressed up to $\hat{\varphi}_g = 8$ (blue full circle). From that point on, the system is followed in a restricted equilibrium, confined to the glass state (full blue line). At high pressure, the glass state becomes marginally stable. Jamming is reached around $\hat{\varphi}_j \approx 10$. The thick lines indicate the specific glass we follow in this paper. Other glasses corresponding to different $\hat{\varphi}_g$ (different compression rates) are plotted with thinner lines.

jams at a density $\hat{\varphi}_j \approx 10$. The phase diagram of Fig. 1 qualitatively agrees with $3d$ numerical simulations [37].

Stress-strain curves.—The glass prepared at $\hat{\varphi}_g$ is first adiabatically compressed to $\hat{\varphi} > \hat{\varphi}_g$, and then a shear strain γ is applied. At the *replica symmetric* level [46], the glass-free energy $f_g(\gamma, \hat{\varphi}; \Delta, \Delta_r)$ can be exactly computed in $d \to \infty$ as a function of two order parameters [44]: Δ is the mean square displacement (MSD) in the glass state at $(\hat{\varphi}, \gamma)$, and Δ_r is the relative MSD of a typical configuration of the glass at $(\hat{\varphi}_g, \gamma = 0)$ and a typical configuration of the same glass once followed up to $(\hat{\varphi}, \gamma)$ (see [44] for the precise mathematical definition). Both are obtained by setting the derivatives of f_g to zero. Once Δ, Δ_r are determined, the average reduced pressure p and average stress σ are derivatives of f_g, with respect to $\hat{\varphi}$ and γ, respectively.

All the four quantities p, σ, Δ, and Δ_r are reported in Fig. 2 as functions of γ for several values of $\hat{\varphi}$. We observe a different behavior at lower densities close to $\hat{\varphi}_g = 8$ and at higher densities close to $\hat{\varphi}_j \approx 10$. For lower $\hat{\varphi}$, there is first a linear elastic regime $\sigma \sim \mu \gamma$, followed by a stress overshoot before the system finally yields at $\gamma_y(\hat{\varphi})$. At the mean-field replica-symmetric level, the yielding point is defined by the fact that stress, pressure, Δ, and Δ_r display a square-root singularity; e.g., $p - p_y(\hat{\varphi}) \propto \sqrt{\gamma_y(\hat{\varphi}) - \gamma}$ because yielding is akin to a spinodal: the solution of the stationarity equations for Δ, Δ_r merges with another unphysical solution and disappears in a bifurcationlike manner. Equivalently, the square-root singularity is due to the vanishing of a *longitudinal mode* $\lambda_L \propto d^2 f_g / d\Delta_r^2$ at $\gamma_y(\hat{\varphi})$. It also implies that there is a diverging susceptibility at $\gamma_y(\hat{\varphi})$, related to the fluctuations of Δ_r: $\Delta_r : \chi_L \sim \langle \Delta_r^2 \rangle - \langle \Delta_r \rangle^2 \propto 1/\lambda_L$. For higher $\hat{\varphi}$, instead, we observe that pressure and stress increase fast and both diverge at a shear jamming point $\gamma_j(\hat{\varphi})$, where $\Delta \to 0$ and Δ_r remain finite.

Phase diagram.—In Fig. 3, the shear yielding line $\gamma_y(\hat{\varphi})$ and the shear jamming line $\gamma_j(\hat{\varphi})$ are reported in the $(\hat{\varphi}, \gamma)$ plane for $\hat{\varphi}_g = 8$. We observe a re-entrant shear jamming line moving to lower densities for increasing γ. The shear yielding line γ_y decreases upon increasing $\hat{\varphi}$. It is possible to show analytically that the two lines merge at a critical point $(\hat{\varphi}_c, \gamma_c)$ at which the system is both jammed (because $\Delta = 0$, $p = \infty$, $\sigma = \infty$) and yielding because the longitudinal mode vanishes indicating an instability of Δ_r (which remains finite at the critical point, but has infinite derivative). Note that beyond the yielding point, the solid phase is unstable and the systems starts to flow: a fixed stress σ corresponds to a finite *shear rate* $\dot{\gamma}$. In this regime, the state following formalism is not appropriate (both Δ_r and Δ are formally infinite), and a fully dynamical treatment is needed, which goes beyond the scope of this Letter. We also computed the phase diagram for different values of $\hat{\varphi}_g$ (not shown). We find that the critical density $\hat{\varphi}_c$ moves
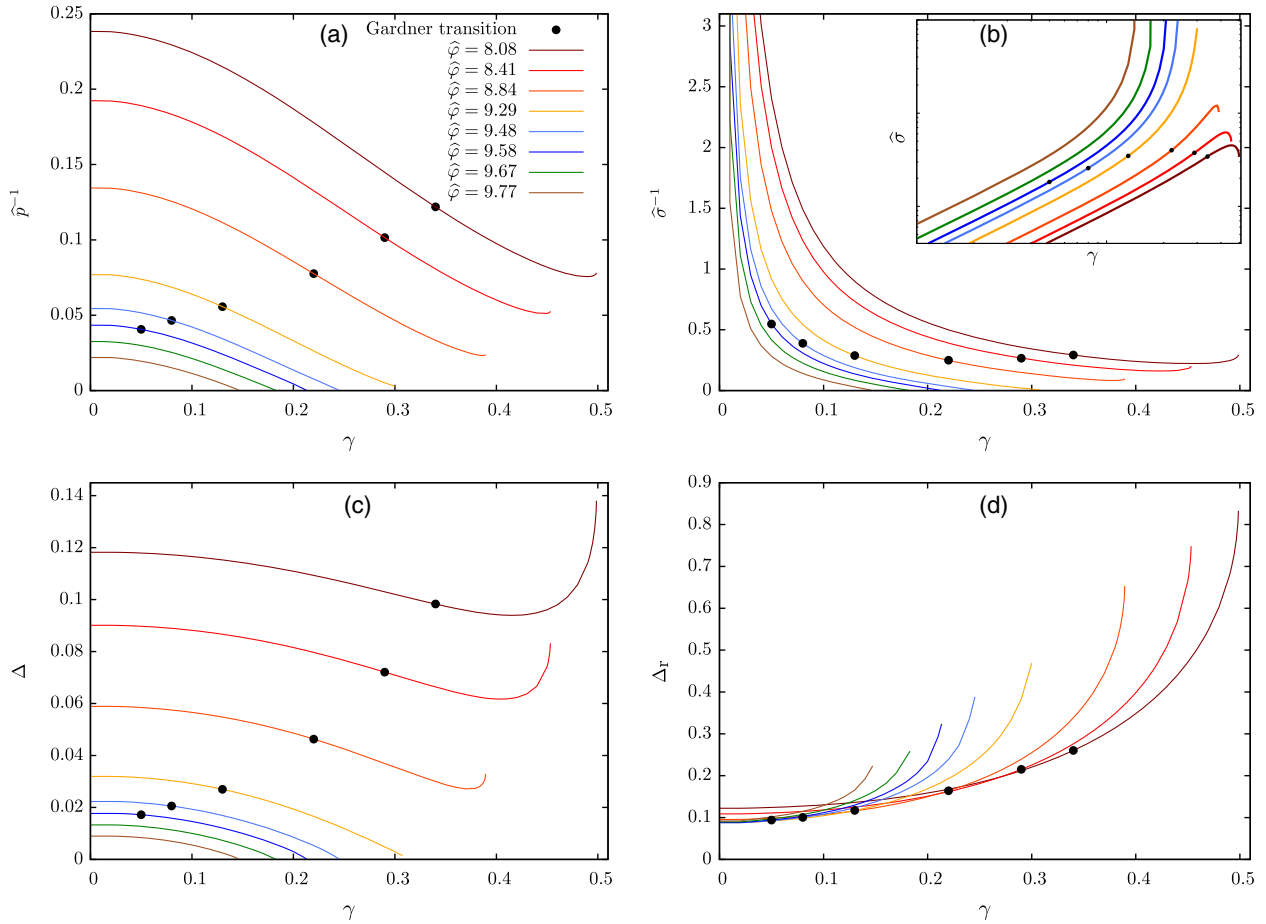
FIG. 2.   Applying adiabatically a shear strain γ on a glass prepared at equilibrium at $\hat{\varphi}_g = 8$ and adiabatically compressed to $\hat{\varphi} \in [\hat{\varphi}_g, \hat{\varphi}_j]$. The black dots along the lines represent the Gardner transition. (a) Inverse reduced pressure $d/p \equiv \hat{p}^{-1}$ vs γ. At lower $\hat{\varphi}$, the pressure is finite until the system yields at $\gamma_y(\hat{\varphi})$. At higher density, the pressure diverges at the shear jamming point $\gamma_j(\hat{\varphi})$. (b) Inverse of the reduced shear stress $\hat{\sigma}^{-1} \equiv d/\sigma$ vs γ. The behavior is very similar to the pressure. At lower $\hat{\varphi}$, the stress overshoots before yielding. At higher $\hat{\varphi}$, the stress diverges at γ_j without any overshoot. The inset shows the behavior of $\hat{\sigma}$ vs γ in log scale. (c) The glass MSD Δ vs γ. At lower $\hat{\varphi}$, Δ remains finite at yielding. At higher $\hat{\varphi}$, Δ vanishes at shear jamming. (d) The MSD Δ_r between the initial equilibrium configuration at $\hat{\varphi}_g$ and the one at $(\hat{\varphi}, \gamma)$. At lower $\hat{\varphi}$, Δ_r remains finite and displays a square-root singularity at yielding, such that $d\Delta_r/d\gamma \to \infty$ for $\gamma \to \gamma_y$. At higher density, Δ_r remains finite at shear jamming with no singularity.

towards $\hat{\varphi}_j$ upon decreasing $\hat{\varphi}_g$, which implies that the shear jamming line shrinks and eventually disappears for poorly equilibrated glassy states with $\hat{\varphi}_g \approx \hat{\varphi}_d$.

Marginal stability.—As previously found in [44,45], the replica symmetric solution used to compute the results of Fig. 2 becomes unstable in a region of the phase diagram delimited by the *Gardner transition line* $\gamma_G(\hat{\varphi})$. Beyond this line, the order parameter Δ becomes a function $\Delta(x)$ defined for $x \in [0, 1]$, and the glass-free energy is a functional $f_g[\gamma, \hat{\varphi}; \Delta(x), \Delta_r]$. The resulting *full replica symmetry breaking* solution [46] is characterized by marginal stability: one of the derivatives of the free energy (the *replicon* mode) is identically vanishing in the marginally stable phase, leading to a diverging susceptibility and the breakdown of standard elasticity [20,29]. The function $\Delta(x)$ and Δ_r are determined by setting the (functional) derivatives of f_g to zero. Although we did not solve the resulting equations numerically (see [45]

for a computation of the stress-strain curves at $\hat{\varphi}_g$), the phase diagram remains qualitatively similar to Fig. 3. Indeed, analytically, we can show the following. (i) Shear jamming is characterized by the vanishing of $\Delta(1)$, the self-MSD of the glass states, which induces a divergence of pressure p and stress σ. On the shear jamming line, the critical properties are the same of the jamming point at zero strain [26]: the interparticle force and gap distributions display power-law behavior, with nontrivial exponents that are constant along the shear jamming line. (ii) Shear yielding is still characterized by the vanishing of $\lambda_L \propto d^2 f_g/d\Delta_r^2$, which induces a divergence of the fluctuations of Δ_r. However, the critical properties on the shear yielding line remain to be understood. (iii) The two lines merge at a critical point where both $\Delta(1) = 0$ and $\lambda_L = 0$.

Comparison with numerics and experiments.—Many experimental and numerical works have studied both shear

yielding and shear jamming. In particular, simulations of athermal systems [25,47–51] and experiments on granular materials [52–54] found a re-entrant shear jamming line.

The phase diagram in our Fig. 3 holds for a specific protocol: a thermal system that is prepared in a well-equilibrated initial state ($\hat{\varphi}_g > \hat{\varphi}_d$) to which compression and shear strain are applied. In a systematic study of a (frictionless) athermal system [25], it has been found that the re-entrance of the shear jamming line is a finite size effect and disappears when $N \to \infty$. There are two possible explanations for this difference. First, it could be due to the lack of initial equilibration of the samples used in [25], which are prepared by quenching instantaneously from infinite temperature: this is consistent with our finding that poorly equilibrated thermal systems do not display shear jamming. Also, while for thermal hard spheres (any $T > 0$), entropic forces stabilize the solid phase in the region delimited by the shear yielding and shear jamming lines in Fig. 3, athermal systems ($T = 0$) below jamming are not rigid (at least for small γ) because both the pressure $P = Tp$ and the stress $\Sigma = T\sigma$ vanish identically at $T = 0$. It is thus possible that they have very different dynamics upon application of shear strain [55], in which case it would be difficult to compare athermal system with our theory. Additional numerical simulations are needed to clarify this issue.
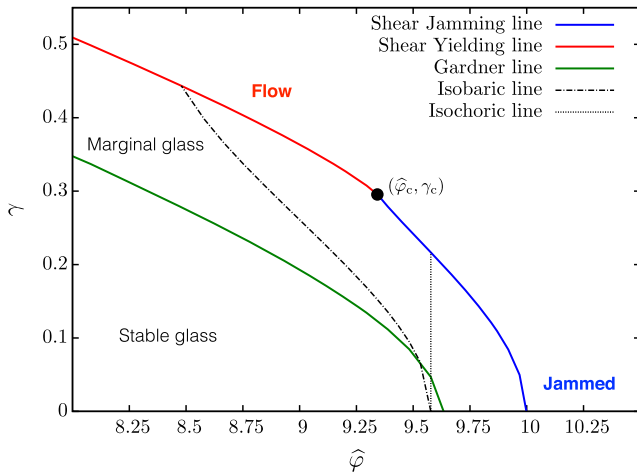

FIG. 3. Phase diagram of the glass prepared in equilibrium at $\hat{\varphi}_g = 8$ and followed adiabatically at density $\hat{\varphi} > \hat{\varphi}_g$ and shear strain γ. The shear jamming line $\gamma_j(\hat{\varphi})$ and the shear yielding line $\gamma_y(\hat{\varphi})$ are plotted. The two lines merge at a critical point $(\hat{\varphi}_c, \gamma_c)$. At this special point, yielding happens at infinite pressure or strain. For $\hat{\varphi} \lesssim \hat{\varphi}_c$, yielding happens at $\gamma \sim \gamma_c$ with extremely large pressure or strain. The vertical dotted line is the isochoric line of a glass prepared at $\hat{\varphi} > \hat{\varphi}_c$ and then strained at fixed volume until it shear jams. The dotted-dashed line represents the isobaric line of a glass prepared at the same initial packing fraction, but then strained at fixed pressure. The shear jamming transition is thus avoided and the glass yields for sufficiently high strains.

Granular materials under tapping could instead be equivalent to thermal systems and display a re-entrance that persists for $N \to \infty$, but a finite-size study has not been performed in this case [52–54]. Also, the results of [56,57] on shear yielding support the idea that this transition is similar to a spinodal point in presence of disorder. A more direct comparison can be made between our theory and very recent simulations of thermal hard spheres under shear [58]. Our predictions are qualitatively compatible with these numerical results. However, none of these studies have investigated the coalescence of the shear yielding and shear jamming lines at $(\hat{\varphi}_c, \gamma_c)$ nor the plastic dynamics around the critical point, which are the most interesting results of this work.

Conclusions.—We investigated the phase diagram of a dense hard sphere glass, prepared in equilibrium at $\hat{\varphi}_g > \hat{\varphi}_d$ and followed adiabatically to density $\hat{\varphi}$ and shear strain γ. The phase diagram in the $(\hat{\varphi}, \gamma)$ plane (Fig. 3) generically displays a shear yielding line when $\hat{\varphi} \gtrsim \hat{\varphi}_g$ and a shear jamming line when $\hat{\varphi} \lesssim \hat{\varphi}_j$. The two lines merge at a critical point, around which the system yields at extremely large pressure and shear stress.

Although our results are derived in a mean-field setting, we expect that they describe accurately the critical exponents associated to the shear jamming line in finite dimensions, as it is the case for $\gamma = 0$ [24,26]. Indeed, the shear jamming line has the same critical properties of the isotropic jamming transition [25]. On the contrary, even at the mean-field level, the critical properties of the shear yielding line are not fully understood because this line falls in a region where the glass is marginally stable and a full replica symmetry breaking scheme is needed [45]. Moreover, because the yielding transition is a spinodal point in presence of disorder, it cannot be strictly described by mean field in any dimension [59,60]. A detailed characterization of the yielding transition is thus a very difficult task and it is certainly a very important line for future research. However, at the critical point $(\hat{\varphi}_c, \gamma_c)$, we conjecture that the system sizes where finite d corrections become important diverge, so that the mean-field theory of the yielding transition can likely become exact close to $(\hat{\varphi}_c, \gamma_c)$. The plastic dynamics around $(\hat{\varphi}_c, \gamma_c)$ are expected to be strongly different from the one of soft glasses. Its analytical and numerical investigation is another very interesting subject for future work. Systematic numerical [58] and experimental [61] investigation of the phase diagram in Fig. 3 will be of great help to fully understand the interplay of yielding and jamming in amorphous solids.

[1] A. Argon and H. Kuo, Mater. Sci. Eng. **39**, 101 (1979).

[2] M. L. Falk and J. S. Langer, Phys. Rev. E **57**, 7192 (1998).

[3] P. Schall, D. A. Weitz, and F. Spaepen, Science **318**, 1895 (2007).

[4] J.-L. Barrat and A. Lemaître, in *Dynamical Heterogeneities in Glasses, Colloids, and Granular Media*, edited by L. Berthier, G. Biroli, J.-P. Bouchaud, L. Cipelletti, and W. van Saarloos (Oxford University Press, Oxford, 2011).

[5] D. Rodney, A. Tanguy, and D. Vandembroucq, Model. Simul. Mater. Sci. Eng. **19**, 083001 (2011).

[6] F. Puosi, J. Rottler, and J.-L. Barrat, Phys. Rev. E **94**, 032604 (2016).

[7] A. K. Dubey, H. G. E. Hentschel, I. Procaccia, and M. Singh, Phys. Rev. B **93**, 224204 (2016).

[8] P. Sollich, F. Lequeux, P. Hébraud, and M. E. Cates, Phys. Rev. Lett. **78**, 2020 (1997).

[9] P. Hébraud and F. Lequeux, Phys. Rev. Lett. **81**, 2934 (1998).

[10] E. Agoritsas, E. Bertin, K. Martens, and J.-L. Barrat, Eur. Phys. J. E **38**, 71 (2015).

[11] J. Lin and M. Wyart, Phys. Rev. X **6**, 011005 (2016).

[12] C. S. O'Hern, S. A. Langer, A. J. Liu, and S. R. Nagel, Phys. Rev. Lett. **88**, 075507 (2002).

[13] G. Parisi and F. Zamponi, Rev. Mod. Phys. **82**, 789 (2010).

[14] S. Torquato and F. H. Stillinger, Rev. Mod. Phys. **82**, 2633 (2010).

[15] M. Wyart, Phys. Rev. Lett. **109**, 125502 (2012).

[16] E. Lerner, G. During, and M. Wyart, Soft Matter **9**, 8252 (2013).

[17] E. DeGiuli, E. Lerner, C. Brito, and M. Wyart, Proc. Natl. Acad. Sci. U.S.A. **111**, 17054 (2014).

[18] G. Combe and J.-N. Roux, Phys. Rev. Lett. **85**, 3628 (2000).

[19] E. Lerner, E. DeGiuli, G. Düring, and M. Wyart, Soft Matter **10**, 5085 (2014).

[20] G. Biroli and P. Urbani, Nat. Phys. **12**, 1130 (2016).

[21] S. Franz and S. Spigler, arXiv:1608.01265.

[22] M. Wyart, L. E. Silbert, S. R. Nagel, and T. S. Witten, Phys. Rev. E **72**, 051306 (2005).

[23] C. Brito and M. Wyart, J. Chem. Phys. **131**, 024504 (2009).

[24] E. Lerner, G. Düring, and M. Wyart, Europhys. Lett. **99**, 58003 (2012).

[25] M. Baity-Jesi, C. P. Goodrich, A. J. Liu, S. R. Nagel, and J. P. Sethna, arXiv:1609.00280.

[26] P. Charbonneau, J. Kurchan, G. Parisi, P. Urbani, and F. Zamponi, Nat. Commun. **5**, 3725 (2014).

[27] P. Charbonneau, E. I. Corwin, G. Parisi, and F. Zamponi, Phys. Rev. Lett. **109**, 205501 (2012).

[28] T. R. Kirkpatrick and P. G. Wolynes, Phys. Rev. A **35**, 3072 (1987).

[29] P. Charbonneau, J. Kurchan, G. Parisi, P. Urbani, and F. Zamponi, arXiv:1605.03008.

[30] P. Charbonneau, Y. Jin, G. Parisi, and F. Zamponi, Proc. Natl. Acad. Sci. U.S.A. **111**, 15025 (2014).

[31] M. Skoge, A. Donev, F. H. Stillinger, and S. Torquato, Phys. Rev. E **74**, 041127 (2006).

[32] P. Charbonneau, A. Ikeda, J. A. van Meel, and K. Miyazaki, Phys. Rev. E **81**, 040501 (2010).

[33] G. Brambilla, D. El Masri, M. Pierno, L. Berthier, L. Cipelletti, G. Petekidis, and A. B. Schofield, Phys. Rev. Lett. **102**, 085703 (2009).

[34] T. S. Grigera and G. Parisi, Phys. Rev. E **63**, 045102 (2001).

[35] S. Singh, M. Ediger, and J. J. de Pablo, Nat. Mater. **12**, 139 (2013).

[36] L. Berthier, D. Coslovich, A. Ninarello, and M. Ozawa, Phys. Rev. Lett. **116**, 238002 (2016).

[37] L. Berthier, P. Charbonneau, Y. Jin, G. Parisi, B. Seoane, and F. Zamponi, Proc. Natl. Acad. Sci. U.S.A. **113**, 8397 (2016).

[38] S. F. Swallen, K. L. Kearns, M. K. Mapes, Y. S. Kim, R. J. McMahon, M. D. Ediger, T. Wu, L. Yu, and S. Satija, Science **315**, 353 (2007).

[39] W. Götze, J. Phys. Condens. Matter **11**, A1 (1999).

[40] T. Maimbourg, J. Kurchan, and F. Zamponi, Phys. Rev. Lett. **116**, 015902 (2016).

[41] S. Franz and G. Parisi, J. Phys. I France **5**, 1401 (1995).

[42] F. Krzakala and L. Zdeborová, Europhys. Lett. **90**, 66002 (2010).

[43] F. Krzakala and L. Zdeborová, J. Phys. Conf. Ser. **473**, 012022 (2013).

[44] C. Rainone, P. Urbani, H. Yoshino, and F. Zamponi, Phys. Rev. Lett. **114**, 015701 (2015).

[45] C. Rainone and P. Urbani, J. Stat. Mech. Theor. Exp. (**2016**) 053302 (2016).

[46] M. Mézard, G. Parisi, and M. A. Virasoro, *Spin Glass Theory and Beyond* (World Scientific, Singapore, 1987).

[47] C. Heussinger and J.-L. Barrat, Phys. Rev. Lett. **102**, 218303 (2009).

[48] C. Heussinger, P. Chaudhuri, and J.-L. Barrat, Soft Matter **6**, 3050 (2010).

[49] R. Pastore, M. Pica Ciamarra, and A. Coniglio, Philos. Mag. **91**, 2006 (2011).

[50] R. Seto, R. Mari, J. F. Morris, and M. M. Denn, Phys. Rev. Lett. **111**, 218301 (2013).

[51] H. Vinutha and S. Sastry, Nat. Phys. **12**, 578 (2016).

[52] R. Candelier and O. Dauchot, Phys. Rev. Lett. **103**, 128001 (2009).

[53] D. Bi, J. Zhang, B. Chakraborty, and R. Behringer, Nature (London) **480**, 355 (2011).

[54] A. Fall, N. Huang, F. Bertrand, G. Ovarlez, and D. Bonn, Phys. Rev. Lett. **100**, 018301 (2008).

[55] A. Ikeda, L. Berthier, and P. Sollich, Phys. Rev. Lett. **109**, 018301 (2012).

[56] P. K. Jaiswal, I. Procaccia, C. Rainone, and M. Singh, Phys. Rev. Lett. **116**, 085501 (2016).

[57] E. Tjhung and L. Berthier, arXiv:1607.01734.

[58] Y. Jin and H. Yoshino, arXiv:1610.07301.

[59] S. Franz, G. Parisi, F. Ricci-Tersenghi, and T. Rizzo, Eur. Phys. J. E **34**, 102 (2011).

[60] S. K. Nandi, G. Biroli, and G. Tarjus, Phys. Rev. Lett. **116**, 145701 (2016).

[61] A. Seguin and O. Dauchot, Phys. Rev. Lett. **117**, 228001 (2016).